2019 3rd International Conference on Recent Advances in Signal Processing, Telecommunications & Computing (SigTelCom)

A Rank-Deficient and Sparse Penalized Optimization Model for Compressive Indoor Radar Imaging

Van Ha Tang and Van-Giang Nguyen
Faculty of Information Technology, Le Quy Don Technical University,
236 Hoang Quoc Viet Street, Hanoi, Vietnam
Email: hatv@lqdtu.edu.vn, giangnv@mta.edu.vn

***Abstract*—This paper proposes a rank-deficient and sparse penalized optimization method for addressing the problem of through-wall radar imaging (TWRI) in the presence of structured wall clutter. Compressive TWRI enables fast data collection and accurate target localization, but faces with the challenges of incomplete data measurements and strong wall clutter. This paper handles these challenges by formulating the task of wall-clutter removal and target image reconstruction as a joint rank-deficient and sparse regularized minimization problem. In this problem, the rank-deficient regularization is used to capture the low-dimensional structure of the wall signals and the sparse penalty is employed to represent the image of the desired targets. We develop a proximal gradient-based algorithm to solve the large-scale optimization problem, which simultaneously removes unwanted wall clutter and reconstruct an image of indoor targets. Real radar datasets are used to validate the effectiveness of the proposed rank-deficient and sparse regularized optimization approach.**

I. Introduction

Through-wall radar (TWR) imaging has emerged as a powerful technology for sensing through walls and opaque structures. It has several potential applications, such as locating victims buried under collapsed buildings, recognizing hostages in police missions, and detecting enemy forces in military operations [1]–[3]. However, TWRI faces strong wall clutter and unwanted interferences, which cause target detection very difficult. Although several studies have been developed to tackle these challenges, there is a high demand for efficient approaches to mitigate wall clutter and provide a high-resolution image of behind-wall targets.

Early TWRI methods form an image of indoor targets by employing backprojection techniques, such as delay-and-sum beamforming [2], which are effective for image formation provided that all antennas and frequencies are used. This condition, however, leads to prolonged data acquisition and ineffective system storage. To enable high-quality imaging and fast data collection, several studies [4]–[6] have been proposed based on compressive sensing (CS) framework [7]. In these methods, the task of image reconstruction is cast as an ℓ_1-regularized optimization problem. If wall clutter has been completely removed prior to image reconstruction, the ℓ_1-regularized methods are suitable. However, in the presence of wall clutter, using directly the ℓ_1-penalized methods recovers only the strong wall-clutter pixels and thereby not revealing the targets. The reason is that the presence of unwanted wall reflections overwhelms target signals, making target detection impossible.

Recent CS-based approaches have investigated target image formation in conjunction with wall clutter mitigation. These techniques typically comprise two major stages [8]–[11]. The first stage aims to remove wall clutter by using techniques, such as spatial filtering [12], subspace projection [13], followed by an ℓ_1 minimization for image reconstruction. Note that because such clutter mitigation techniques are not effective for missing-measurement cases, antenna signal reconstruction needs to be conducted before applying clutter mitigation techniques. In other words, these existing approaches detect targets via multistage of signal representation, wall-clutter suppression, and target-image formation, but these stages are conducted independently.

This paper introduces a rank-deficient and sparse representation approach for simultaneously solving the problem of wall clutter removal and target image reconstruction in compressive TWRI. The proposed model exploits the prior knowledge of the low-dimensional structure of wall clutter and the sparsity of the target scene. The former characteristic is because the wall signals along the antenna array are highly correlated. As a result, if the wall antenna signals are arranged as columns of a matrix, this matrix is rank-deficient. The sparseness of the target image holds true if the wall component has been well-captured. The task of clutter mitigation and image reconstruction is formulated as a nuclear and ℓ_1-norm regularized least squares (LS) minimization problem. The LS term bounds the measurement error; the nuclear-norm penalty is a convex relaxation for the rank-deficient property of the wall-clutter matrix, and the ℓ_1-norm promotes the sparsity of the target image. This paper introduces an iterative shrinkage algorithm, based on the first-order proximal gradient (PG) method, to solve the joint nuclear and ℓ_1 regularized LS problem, yielding a matrix containing wall-clutter and an image of indoor targets simultaneously.

The paper is structured as follows. Section II briefly presents TWR signal model, and Section III describes the rank-deficient and sparse penalized LS optimization method for TWRI. Experimental evaluation is given in Section IV and finally, Section V concludes the paper with noticeable remarks.

II. Through-wall radar signal model

In this section, we present briefly the mathematical signal model of a radar system that uses stepped-frequency and

This research is funded by Vietnam National Foundation for Science and Technology Development (NAFOSTED) under grant number 102.01-2017.307.

978-1-5386-7963-0/19/$31.00 ©2019 IEEE

operates in a monostatic mode to image a scene behind a wall. The scene supposes to contain P targets, which are sensed by placing a transceiver along the line parallel to the wall, synthesizing an N-element linear antenna array. Each antenna uses an M-step frequency signal to image the scene. The received signal $z_{m,n}$ for the m-th frequency at the n-th antenna is superimposed by the wall clutter (reverberations) $z^w_{m,n}$, target signal $z^t_{m,n}$, and noise $\upsilon_{m,n}$:

$$z_{m,n} = z^w_{m,n} + z^t_{m,n} + \upsilon_{m,n}. \tag{1}$$

The wall component $z^w_{m,n}$ is modeled as

$$z^w_{m,n} = \sum_{r=1}^{R} \sigma_w a_r e^{-j2\pi f_m \tau^r_{n,w}}. \tag{2}$$

In this model, σ_w represents the wall reflectivity, R is the total number of reverberations due to the wall, a_r is the factor accounting for the path loss of the r-th wall reverberation, and $\tau^r_{n,w}$ is the r-th wall return travel delay. The target scatterer can be expressed as

$$z^t_{m,n} = \sum_{p=1}^{P} \sigma_p e^{-j2\pi f_m \tau_{n,p}}, \tag{3}$$

where σ_p denotes the p-th target reflectivity, and $\tau_{n,p}$ measures the two-way signal travel time between the n-th antenna and the p-th target.

To form a target image, the target space is divided into Q pixels as a rectangular grid along the crossrange and downrange directions. The value s_q is considered as a weighted indicator function used to represent the p-th target reflectivity:

$$s_q = \begin{cases} \sigma_p, & \text{if the } p\text{-th target occupies the } q\text{-th pixel;} \\ 0, & \text{otherwise.} \end{cases} \tag{4}$$

In TWRI, the targets appear as clusters consisting of points populated accurately on the image-pixel locations. Arranging measurements collected at the n-th antenna, $\mathbf{z}^t_n = [z^t_{1,n}, \ldots, z^t_{M,n}]^T$, from (3), we can relate the measurement-vector $\mathbf{z}^t_n$ to the image scene $\mathbf{s} = [s_1, \ldots, s_Q]^T$, via a dictionary matrix $\mathbf{\Psi}_n \in \mathbb{C}^{M\times Q}$:

$$\mathbf{z}^t_n = \mathbf{\Psi}_n\, \mathbf{s}. \tag{5}$$

The (m,q)-th entry of $\mathbf{\Psi}_n \in \mathbb{C}^{M\times Q}$ is defined as $\psi_n(m,q) = \exp(-j2\pi f_m \tau_{n,q})$. Note that to focus the target image, TWRI considers the signal delay penetrating through the wall. Details of the computation for the focusing delay, $\tau_{n,q}$, from the n-th antenna to the q-th pixel are given in [2, 14, 15]. Arranging all data measurements, $\mathbf{z}^t = [(\mathbf{z}^t_1)^T, \ldots, (\mathbf{z}^t_N)^T]^T$, and dictionary matrices, $\mathbf{\Psi} = [\mathbf{\Psi}^T_1, \ldots, \mathbf{\Psi}^T_N]^T$, for N antennas, we have the linear model,

$$\mathbf{z}^t = \mathbf{\Psi}\, \mathbf{s}. \tag{6}$$

From (6), if the target signal $\mathbf{z}^t_l$ is available, the target image $\mathbf{s}$ can be estimated using DS beamforming or direct CS technique. The DS beamforming generates the image $\mathbf{s}$ by premultiplying the target signal $\mathbf{z}^t_l$ with the adjoint operator $\mathbf{\Psi}^H$:

$$\mathbf{s} = \mathbf{\Psi}^H\, \mathbf{z}^t. \tag{7}$$

The direct CS promotes the sparsity of $\mathbf{s}$ and obtains the image by solving an ℓ_1-regularization problem:

$$\mathbf{s} = \arg\min_{\mathbf{s}} \left\{ \frac{1}{2} \|\mathbf{z}^t - \mathbf{\Psi}\, \mathbf{s}\|^2_2 + \lambda \|\mathbf{s}\|_1 \right\}, \tag{8}$$

where λ is a positive parameter. However, it is noted from (1) that the target signal $\mathbf{z}^t$ does not exist for image formation. Instead, the radar system receives the radar signal $\mathbf{z}$, in which the wall return $\mathbf{z}^w$ dominates the target component $\mathbf{z}^t$, plus noise $\boldsymbol{\upsilon}$. Since the wall component $\mathbf{z}^w$ overwhelms target signal $\mathbf{z}^t$, the image $\mathbf{s}$ obtained from (7) or (8) reveals wall clutter pixels only. Hence, before reconstruction of the target image, wall clutter mitigation needs to be performed. This task, however, is even more challenging under generic CS contexts in which not full data volume is available. This paper proposes a rank-deficient and sparsity approach that solves the problem of wall clutter mitigation and target image reconstruction jointly in the CS operations.

III. Rank-deficient and sparse regularized TWRI

A. Nuclear and ℓ_1-norm regularized LS problem

Arranging the radar signals, wall clutter, target signals, and noise collected for all M frequencies by N antenna positions, we obtain $\mathbf{Z} = [z_{m,n}]$, $\mathbf{Z}^w = [z^w_{m,n}]$, $\mathbf{Z}^t = [z^t_{m,n}]$, and $\mathbf{\Upsilon} = [\upsilon_{m,n}]$. By doing so, we convert Eq. (1) into a matrix-form model,

$$\mathbf{Z} = \mathbf{Z}^w + \mathbf{Z}^t + \mathbf{\Upsilon}. \tag{9}$$

The signal model in (9) represents TWRI operations in the full sensing mode. In CS, however, only a subset of K samples ($K \ll M \times N$) is acquired. This CS data acquisition can be modeled via a sensing matrix $\mathbf{\Phi} \in \mathbb{R}^{K\times MN}$; $\mathbf{\Phi}$ has only one non-zero element (equal to 1) in each row which indicates the used frequency for a selected antenna. Using $\mathbf{\Phi}$, we obtain a reduced measurement vector $\mathbf{y} \in \mathbb{C}^K$ as

$$\mathbf{y} = \mathbf{\Phi}\, \mathrm{vec}(\mathbf{Z}) = \mathcal{A}(\mathbf{Z}). \tag{10}$$

In (10), $\mathrm{vec}(\mathbf{Z})$ is the operator that forms a long column vector by stacking the columns in $\mathbf{Z}$; $\mathbf{Z}$ can be obtained from $\mathbf{y}$ as $\mathbf{Z} = \mathrm{mat}(\mathbf{\Phi}^\dagger \mathbf{y}) = \mathcal{A}^*(\mathbf{y})$. Here, † is the pseudo-inverse operator and mat is the operator converting a column vector having MN entries into an $M \times N$ matrix. Combining (9) and (10) yields

$$\mathbf{y} = \mathbf{\Phi}\mathrm{vec}(\mathbf{Z}) = \mathbf{\Phi}\mathrm{vec}(\mathbf{Z}^w) + \mathbf{\Phi}\mathrm{vec}(\mathbf{Z}^t) + \mathbf{\Phi}\mathrm{vec}(\mathbf{\Upsilon}). \tag{11}$$

Now, using vector $\mathbf{y}$ and exploiting the model that relates the target signal and the image in (6), $\mathrm{vec}(\mathbf{Z}^t) = \mathbf{z}^t = \mathbf{\Psi}\, \mathbf{s}$, we can attain the wall component $\mathbf{Z}^w$ and the image $\mathbf{s}$ as the solution to the following optimization problem:

$$\begin{aligned} \min_{Z^w, s} \quad & \|\mathbf{Z}^w\|_* + \lambda \|\mathbf{s}\|_1 \\ \text{subject to} \quad & \|\mathbf{y} - [\mathcal{A}(\mathbf{Z}^w) + \mathbf{\Phi}\, \mathbf{\Psi}\, \mathbf{s}]\|^2_2 \le \epsilon. \end{aligned} \tag{12}$$

Here, $\|\mathbf{Z}^w\|_*$ is the nuclear-norm defined as the sum of the singular values of $\mathbf{Z}^w$, $\|\mathbf{s}\|_1$ is the ℓ_1-norm defined as the sum of absolute entries of $\mathbf{s}$, λ is a regularization parameter, and

ϵ is a noise bound. Problem (12) can be handled efficiently by casting into the standard Lagrangian form:

$$\min_{Z^w,s}\{f(\mathbf{Z}^w,\mathbf{s}) \equiv \frac{1}{2}\left\|\mathbf{y}-[\mathcal{A}(\mathbf{Z}^w)+\mathbf{\Phi}\,\mathbf{\Psi}\,\mathbf{s}]\right\|_2^2 + \gamma(\left\|\mathbf{Z}^w\right\|_* + \lambda\left\|\mathbf{s}\right\|_1)\}. \quad (13)$$

Convex theory has proved that the solutions to (12) and (13) are equivalent if γ and ϵ obey certain relationships [16].

B. Proximal gradient algorithm

We propose an effective algorithm to minimize $f(\mathbf{Z}^w,\mathbf{s})$ in (13), producing the wall clutter $\mathbf{Z}^w$ and target image $\mathbf{s}$ simultaneously, based on the generic proximal gradient (PG) technique. This PG technique minimizes an objective function $f(\mathbf{x})$ formed from two convex functions $g(\mathbf{x})$ and $h(\mathbf{x})$:

$$\min_{\mathbf{x}}\{f(\mathbf{x}) \equiv g(\mathbf{x}) + \lambda\, h(\mathbf{x})\}. \quad (14)$$

Here, $g(\mathbf{x})$ is smooth and differentiable, as the case of the quadratic term in (13), whereas $h(\mathbf{x})$ can be nonsmooth, as the sum of the nuclear and ℓ_1 norm terms in (13). Generally, dealing with Problem (14) is complicated. PG overcomes this issue by the objective function decomposition via an *iterative technique*. Let $\mathbf{x}_k$ denote a solution estimated by the k-th iteration. Using $\mathbf{x}_k$ and computing an auxiliary point,

$$\mathbf{u}_k = \mathbf{x}_k - \alpha\nabla g(\mathbf{x}_k), \quad (15)$$

we can obtain the next estimate $\mathbf{x}_{k+1}$ by solving

$$\mathbf{x}_{k+1} = \arg\min_{\mathbf{x}}\left\{\frac{1}{2}\left\|\mathbf{u}_k-\mathbf{x}\right\|_2^2 + \lambda\alpha\, h(\mathbf{x})\right\}. \quad (16)$$

In (15), $\nabla g(\mathbf{x}_k)$ is the gradient of $g(\mathbf{x})$ computed using $\mathbf{x}_k$. Let C be the Lipschitz constant of the ∇g. This iterative algorithm converges if $0 < \alpha \le 1/C$. Special instances of this generic PG method include proximal forward-backward splitting [17] or fast shrinkage algorithm [18].

We apply the PG scheme in (15)–(16) to minimize Problem (13). Let $(\mathbf{Z}_k^w, \mathbf{s}_k)$ denote an estimate of the wall component and target image at the k-th iteration. The next estimates are obtained by solving

$$(\mathbf{Z}_{k+1}^w,\mathbf{s}_{k+1}) = \arg\min_{\mathbf{Z}^w,\mathbf{s}}\{\frac{1}{2}\|\mathbf{Z}_k-\mathbf{Z}^w-\mathcal{A}^*(\mathbf{\Phi}\,\mathbf{\Psi}\,\mathbf{s})\|_F^2 + \alpha\gamma\|\mathbf{Z}^w\|_* + \alpha\gamma\lambda\left\|\mathbf{s}\right\|_1\}, \quad (17)$$

where $\mathbf{Z}_k$ plays the role of $\mathbf{u}_k$ in (15),

$$\mathbf{Z}_k = \mathbf{Z}_k^w + \mathcal{A}^*(\mathbf{\Phi}\,\mathbf{\Psi}\,\mathbf{s}_k) - \alpha\mathcal{A}^*(\mathcal{A}(\mathbf{Z}_k^w) + \mathbf{\Phi}\,\mathbf{\Psi}\,\mathbf{s}_k - \mathbf{y}), \quad (18)$$

and $\alpha \in (0, 1/\|\mathbf{\Phi}\|_2^2]$ for convergence. Hereafter, $\|\mathbf{\Phi}\|_2$ is the spectral norm of matrix defined as the maximum singular value of $\mathbf{\Phi}$. Using the variable splitting technique, we can handle Problem (17) via addressing two subproblems:

$$\mathbf{Z}_{k+1}^w = \arg\min_{\mathbf{Z}^w}\left\{\frac{1}{2}\|\mathbf{Z}_k-\mathbf{Z}^w-\mathcal{A}^*(\mathbf{\Phi}\mathbf{\Psi}\mathbf{s}_k)\|_F^2+\alpha\gamma\|\mathbf{Z}^w\|_*\right\}, \quad (19)$$

$$\mathbf{s}_{k+1} = \arg\min_{\mathbf{s}}\left\{\frac{1}{2}\|\mathbf{Z}_k-\mathbf{Z}_{k+1}^w-\mathcal{A}^*(\mathbf{\Phi}\mathbf{\Psi}\mathbf{s})\|_F^2+\alpha\gamma\lambda\|\mathbf{s}\|_1\right\}. \quad (20)$$

Subproblems (19) and (20) can be handled efficiently via shrinkage/soft-thresholding techniques. Particularly, the nuclear-norm penalized LS problem (19) is solved using the *singular value soft-thresholding* (SVT) technique [19]. The solution is obtained by applying an SVT operator, $\mathcal{S}_{\alpha\gamma}(\cdot)$, to the input matrix:

$$\mathbf{Z}_{k+1}^w = \mathcal{S}_{\alpha\gamma}(\mathbf{Z}_k - \mathcal{A}^*(\mathbf{\Phi}\,\mathbf{\Psi}\,\mathbf{s}_k)). \quad (21)$$

The SVT $\mathcal{S}_\tau(\mathbf{Z})$ is regarded as a nonlinear function applying a shrinkage operator of level τ to the singular values of $\mathbf{Z}$. The shrinkage or soft-thresholding operator is defined as

$$\mathcal{T}_\tau(x) = \mathrm{sign}(x)\max(|x|-\tau,0) = \tfrac{x}{|x|}\max(|x|-\tau,0). \quad (22)$$

Once $\mathcal{T}_\tau(\cdot)$ is defined, $\mathcal{S}_\tau(\mathbf{Z})$ is given by

$$\mathcal{S}_\tau(\mathbf{Z}) = \mathbf{U}\,\mathcal{T}_\tau(\mathbf{\Lambda})\,\mathbf{V}^H, \quad (23)$$

where $\mathbf{Z} = \mathbf{U}\,\mathbf{\Lambda}\,\mathbf{V}^H$ is the singular value decomposition of $\mathbf{Z}$. For matrices, $\mathcal{T}_\tau(\cdot)$ is applied to each element (entrywise).

The ℓ_1 regularized minimization (20) is solved by using the splitting technique (15)–(16):

$$\mathbf{s}_{k+1} = \arg\min_{\mathbf{s}}\left\{\frac{1}{2}\left\|\mathbf{b}-\mathbf{s}\right\|_2^2 + \beta\alpha\gamma\lambda\left\|\mathbf{s}\right\|_1\right\}, \quad (24)$$

where $\mathbf{b}$ is defined as

$$\mathbf{b} = \mathbf{s}_k - \beta\mathbf{\Psi}^H(\mathbf{\Phi}\,\mathbf{\Psi}\,\mathbf{s}_k - \mathcal{A}(\mathbf{Z}_k - \mathbf{Z}_{k+1}^w)), \quad (25)$$

for $0 < \beta \le 1/||\mathbf{\Psi}||_2^2$. Using the proximal mapping [20], we can solve Problem (24) by applying the shrinkage operator to $\mathbf{b}$, yielding the next estimate as

$$\mathbf{s}_{k+1} = \mathcal{T}_{\beta\alpha\gamma\lambda}(\mathbf{b}). \quad (26)$$

The main steps of the algorithm to solve Problem (13) are summarized in Algorithm 1. The input into Algorithm 1 includes the measurement vector $\mathbf{y}$, gradient stepsizes of α, β, regularization parameters γ, λ, and a tolerance tol. Setting values for these parameters is described in Section IV-A.

Algorithm 1: Wall-clutter removal and target-image estimation in compressive TWRI using PG technique.

1) Initialize $\mathbf{Z}_0^w \leftarrow \mathcal{A}^*(\mathbf{y})$, $\mathbf{S}_0 \leftarrow \mathbf{0}$, and $k \leftarrow 0$.
2) Compute gradient evaluation using (18):
$\mathbf{Z}_k \leftarrow \mathbf{Z}_k^w + \mathcal{A}^*(\mathbf{\Phi}\,\mathbf{\Psi}\,\mathbf{s}_k) - \alpha\mathcal{A}^*(\mathcal{A}(\mathbf{Z}_k^w) + \mathbf{\Phi}\,\mathbf{\Psi}\,\mathbf{s}_k - \mathbf{y})$.
3) Perform wall clutter estimation using (21):
$\mathbf{Z}_{k+1}^w \leftarrow \mathcal{S}_{\alpha\gamma}(\mathbf{Z}_k - \mathcal{A}^*(\mathbf{\Phi}\,\mathbf{\Psi}\,\mathbf{s}_k))$.
4) Reconstruct an image of the targets using (26):
$\mathbf{b} \leftarrow \mathbf{s}_k - \beta\mathbf{\Psi}^H(\mathbf{\Phi}\,\mathbf{\Psi}\,\mathbf{s}_k - \mathcal{A}(\mathbf{Z}_k - \mathbf{Z}_{k+1}^w))$,
$\mathbf{s}_{k+1} \leftarrow \mathcal{T}_{\beta\alpha\gamma\lambda}(\mathbf{b})$.
5) Compute the objective function $f(\mathbf{Z}_{k+1}^w, \mathbf{s}_{k+1})$ using (13),
if $\frac{|f(\mathbf{Z}_{k+1}^w,\mathbf{s}_{k+1}) - f(\mathbf{Z}_k^w,\mathbf{s}_k)|}{|f(\mathbf{Z}_k^w,\mathbf{s}_k)|} < \mathrm{tol}$ then terminate,
otherwise increase $k \leftarrow k+1$ and go to Step 2.

IV. Experimental Results

A. Experimental setup

Real radar datasets were collected from a real, shown in in Fig. 1, containing one dihedral target placed behind a wooden wall. This behind-wall scene is sensed by a 81-element linear antenna array synthesized by a monostatic radar system. The radar system transceives a 801-step frequency signal covering the bandwidth of [1–3 GHz]. This stepped-frequency synthetic radar aperture was positioned in front of the 0.16 m-thick wooden wall, at a standoff distance of 1.0 m.

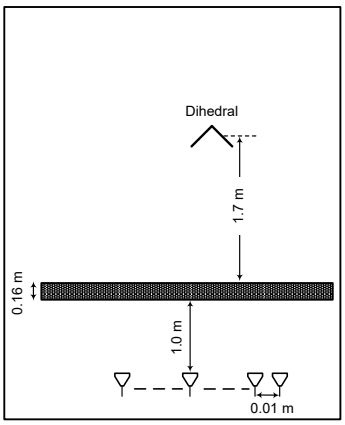

Fig. 1. Layout of the scene with a wooden wall and one dihedral target for TWR data acquisition.

B. Experimental results

This experiment evaluates the proposed rank-deficient and sparse approach and other existing CS-based imaging methods under generic CS operations where both antennas and frequencies are highly compressed. CS radar imaging acquired a reduced dataset, instead of full data volume, by randomly selecting only half of the available antennas (41 out of 81). Each antenna employs only 30% (240 out of 801) frequencies, which are randomly sampled. Thus, the used dataset constitutes only 15% of the full data volume. This reduced dataset is used as input into the proposed PG algorithm for clutter mitigation and image reconstruction. Input parameters for the proposed PG algorithm are selected as follows: the gradient stepsizes $\alpha = 1/\|\mathbf{\Phi}\|_2^2$, $\beta = 1/||\mathbf{\Psi}||_2^2$, the regularization parameters $\gamma = 10^{-1}\|\mathcal{A}^*(\mathbf{Y})\|_2$, $\lambda = 7\times 10^{-1}\|(\mathbf{\Phi}\mathbf{\Psi})^H\mathbf{y}\|_\infty$, and the tolerance value $\mathrm{tol}=10^{-4}$. Using the same reduced dataset, we also implement the existing direct CS and multistage CS approaches for comparison. The existing multistage approaches first perform data recovery, then employ a spatial filtering [12] or a subspace projection technique [13] for wall-clutter mitigation, and finally reconstruct a target image by solving the ℓ_1-norm regularized problem in (8).

Fig. 2 depicts the target images reconstructed using different imaging methods. Without clutter removal, the direct CS method forms an image shown in Fig. 2(a). It can be observed that strong wall reverberations overwhelm the desired target and cause target localization impossible. On the other hand, by incorporating a wall clutter migration technique, multistage CS approaches produce target images in which strong wall clutter has been removed, revealing the desired target, as illustrated in Figs. 2(b) and (c). The proposed rank-deficient and sparse yields the image depicted in Fig. 2(d) where the target pixels are further enhanced and clutter regions are alleviated considerably.

The performances of the imaging methods are quantified using the target-to-clutter ratio (TCR). Let A_t and A_c be, respectively, the regions of target and clutter on the reconstructed image I, and let N_t and N_c be, respectively, the number of target and clutter pixels. The TCR (in dB) measures the ratio of the average powers of the target region over the clutter region:

$$\mathrm{TCR} = 10\log_{10}\left(\frac{\frac{1}{N_t}\sum_{q\in A_t}|I_q|^2}{\frac{1}{N_c}\sum_{q\in A_c}|I_q|^2}\right). \tag{27}$$

It is worth noting that the target region is chosen in the vicinity of the true targets, and the clutter region is defined as the entire image, without the target region. The TCR values of the target images, shown in Fig. 2, formed by the different CS-based methods are computed and listed in Table I. As we expect from the visual interpretation, the proposed joint nuclear-norm and ℓ_1-norm approach yields the target image with a TCR value of 26.87 dB, the highest TCR value among those of the evaluated CS-based imaging approaches.

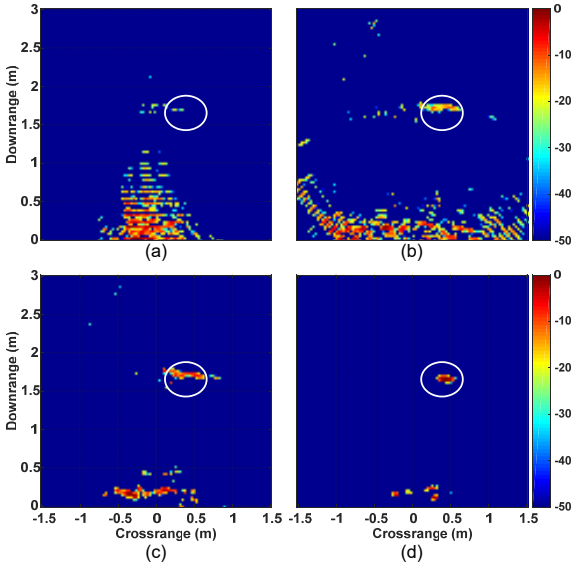

Fig. 2. Images produced by different CS-based wall clutter reduction and target image reconstruction methods with 50% antennas and 30% frequencies (collectively represent only 15% of full measurements): (a) direct ℓ_1-norm minimization without clutter mitigation, (b) multistage CS approach with signal estimation, spatial filtering, and ℓ_1-norm minimization, (c) multistage CS approach with signal estimation, subspace projection, and ℓ_1-norm minimization, and (d) proposed joint nuclear-norm and ℓ_1-norm method.

TABLE I
TARGET-TO-CLUTTER RATIO PERFORMANCES FOR THE IMAGES PRODUCED BY SEVERAL CS-BASED TECHNIQUES WITH 50% ANTENNAS AND 30% FREQUENCIES (COLLECTIVELY REPRESENT ONLY 15% OF FULL MEASUREMENTS).

Clutter mitigation & image formation methods	TCR (dB)
Proposed rank-deficient and sparsity approach	**26.87**
Multistage signal esti. & sub. proj. & ℓ_1 min. [13, 8]	10.62
Multistage signal esti. & spati. filt. & & ℓ_1 min. [12, 8]	-1.55
Direct ℓ_1 min. without clutter mitigation [4, 5]	-15.22

Further insights into the proposed optimization model can be observed from the evolution of the objective function $f(\mathbf{Z}^w, \mathbf{s})$, shown in Fig. 3 and the change of the rank values for the wall component matrix $\mathbf{Z}^w$, shown in Fig. 4. Clearly,

the cost function is monotone-decreasing and converges well after 24 iterations. Likewise, as demonstrated in Fig. 4, the rank value starts at 41 $(\min(240, 41))$ and achieves a value of 1 at the steady-state.

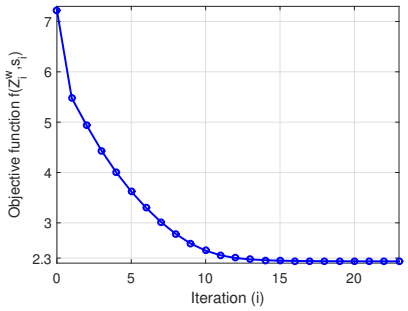

Fig. 3. Evolution of the objective function $f(\mathbf{Z}^w, \mathbf{s})$ during minimization: the cost function value initializes at 7.22, decreases to a local minimum of 2.23 at convergence.

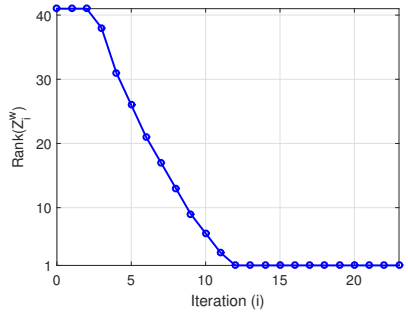

Fig. 4. The rank values of the estimated wall component $\mathbf{Z}^w$ as a function of the number of iterations: the rank decreasing from 41 at first iteration to 1 at convergence.

V. Conclusion

This paper introduced a rank-deficient and sparsity regularized optimization method to address two important problems of wall clutter mitigation and target image formation in compressive indoor radar imaging. We develop the PG-based algorithm to solve the composite nuclear and ℓ_1-penalized minimization problem, removing the wall clutter and yielding the indoor target image. We conducted several experimental evaluations on real radar data and found that exploiting both rank-deficient and sparsity structures improves the accuracy of clutter suppression and target detection even with highly compressed measurements.

Acknowledgments

The authors would like to thank Drs. Abdesselam Bouzerdoum and Son Lam Phung from the Centre of Signal and Information Processing at University of Wollongong, Australia, for providing part of the experimental data.

References

[1] M. G. Amin (Ed.), *Through-The-Wall Radar Imaging*. Boca Raton, FL: CRC Press, 2010.

[2] F. Ahmad, M. G. Amin, and S. A. Kassam, "Synthetic aperture beamformer for imaging through a dielectric wall," *IEEE Trans. Aerosp. and Electron. Syst.*, vol. 41, no. 1, pp. 271–283, Jan. 2005.

[3] V. H. Tang, A. Bouzerdoum, S. L. Phung, and F. H. C. Tivive, "A sparse Bayesian learning approach for through-wall radar imaging of stationary targets," *IEEE Trans. Aerosp. and Electron. Syst.*, vol. 53, no. 5, pp. 2485–2501, Oct. 2017.

[4] Y.-S. Yoon and M. G. Amin, "Compressed sensing technique for high-resolution radar imaging," in *Proc. SPIE: Signal Process., Sensor Fusion, and Target Recognition XVII*, Orlando, FL, Mar. 2008, pp. 69 681A.1– 69 681A.10.

[5] Q. Huang, L. Qu, B. Wu, and G. Fang, "UWB through-wall imaging based on compressive sensing," *IEEE Trans. Geosci. and Remote Sens.*, vol. 48, no. 3, pp. 1408–1415, Mar. 2010.

[6] V. H. Tang, A. Bouzerdoum, and S. L. Phung, "Two-stage through-the-wall radar image formation using compressive sensing," *J. Electron. Imaging*, vol. 22, no. 2, pp. 021 006.1–021 006.10, Apr.–Jun. 2013.

[7] D. L. Donoho, "Compressed sensing," *IEEE Trans. Inf. Theory*, vol. 52, no. 4, pp. 1289–1306, Apr. 2006.

[8] E. Lagunas, M. G. Amin, F. Ahmad, and M. Najar, "Joint wall mitigation and compressive sensing for indoor image reconstruction," *IEEE Trans. Geosci. and Remote Sens.*, vol. 51, no. 2, pp. 891 – 906, Feb. 2013.

[9] V. H. Tang, A. Bouzerdoum, S. L. Phung, and F. H. C. Tivive, "Enhanced wall clutter mitigation for through-the-wall radar imaging using joint Bayesian sparse signal recovery," *Proc. IEEE Int. Conf. Acoust., Speech and Signal Process.*, pp. 7804–7808, Florence, Italy, May 2014.

[10] F. Ahmad, J. Qian, and M. G. Amin, "Wall clutter mitigation using discrete prolate spheroidal sequences for sparse reconstruction of indoor stationary scenes," *IEEE Trans. Geosci. and Remote Sens.*, vol. 53, no. 3, pp. 1549–1557, Mar. 2015.

[11] A. Bouzerdoum, F. H. C. Tivive, and V. H. Tang, "Multi-polarization through-the-wall radar imaging using joint Bayesian compressed sensing," in *IEEE Int. Conf. Digital Signal Process.*, Hong Kong, Aug. 2014, pp. 783–788.

[12] Y.-S. Yoon and M. G. Amin, "Spatial filtering for wall-clutter mitigation in through-the-wall radar imaging," *IEEE Trans. Geosci. and Remote Sens.*, vol. 47, no. 9, pp. 3192–3208, Sept. 2009.

[13] F. H. C. Tivive, A. Bouzerdoum, and M. G. Amin, "A subspace projection approach for wall clutter mitigation in through-the-wall radar imaging," *IEEE Trans. Geosci. and Remote Sens.*, vol. 53, no. 4, pp. 2108–2122, Apr. 2015.

[14] M. G. Amin and F. Ahmad, "Wideband synthetic aperture beamforming for through-the-wall imaging," *IEEE Signal Process. Mag.*, vol. 25, no. 4, pp. 110–113, 2008.

[15] V. H. Tang, A. Bouzerdoum, and S. L. Phung, "Multipolarization through-wall radar imaging using low-rank and jointly-sparse representations," *IEEE Trans. Image Process.*, vol. 27, no. 4, pp. 1763–1776, Apr. 2018.

[16] R. T. Rockafellar, *Convex Analysis*. Princeton Math. Ser. 28, Princeton University Press, Princeton, NJ, 1970.

[17] P. L. Combettes and V. R. Wajs, "Signal recovery by proximal forward-backward splitting," *SIAM J. Multiscale Modeling Simulation*, vol. 4, no. 4, pp. 1168–1200, Nov. 2006.

[18] A. Beck and M. Teboulle, "A fast iterative shrinkage-thresholding algorithm for linear inverse problems," *SIAM J. Imaging Sci.*, vol. 2, no. 1, pp. 183–202, Mar. 2009.

[19] J.-F. Cai, E. J. Candes, and Z. Shen, "A singular value thresholding algorithm for matrix completion," *SIAM J. Optimization*, vol. 20, no. 4, pp. 1956–1982, Mar. 2010.

[20] N. Parikh and S. Boyd, "Proximal algorithms," in *Foundations and Trends in Optimization*, vol. 1, no. 3. Now Publishers Inc, Nov. 2013, pp. 123–231.